Planets in turbulent Disks

Wilhelm Kley
Institute for Astronomy and Astrophysics
Eberhard-Karls-Universität Tübingen
Tübingen, Germany
wilhelm.kley@uni-tuebingen.de

Moritz H.R. Stoll
Institute for Astronomy and Astrophysics
Eberhard-Karls-Universität Tübingen
Tübingen, Germany
moritz.stoll@uni-tuebingen.de

Giovanni Picogna
Universitätssternwarte
University of Munich
München, Germany
picogna@usm.lmu.de

***Abstract*—Planets form in protoplanetary accretion disks around young protostars. These disks are driven by internal turbulence and the gas flow is in general not laminar but has stochastic components. For weakly ionized disks the turbulence can be generated purely hydrodynamically through the vertical shear instability (VSI). Planets, that are forming in such turbulent disks, experience random components in the torques acting on them, that will modify their migration behaviour.**

In this contribution we present results of our study of the impact that a turbulent disk has on an embedded planet. For that purpose we performed three-dimensional hydrodynamical simulations of a locally isothermal disk with embedded planets of various masses. For the lower mass planets (5 and 10 $M_\oplus$) we find that the inward migration rate can be faster than in the laminar case, while for the more massive planets (30 and 100 $M_\oplus$) the results agree well with the laminar results.

***Index Terms*—planet formation, accretion disks, computational astrophysics**

I. Introduction

To simulate planets embedded in turbulent accretion disks our computational domain consists of a 3D section of a disk in spherical polar coordinates (r, θ, ϕ). We will use also cylindrical coordinates (R, Z, ϕ) to describe our setup and the results. We perform hydrodynamical simulations using a locally isothermal equation of state where the temperature is a fixed function of radius

$$T(R) = T_0 \left(\frac{R}{R_\mathrm{p}}\right)^q ,$$

and vertically isothermal. Here we use $q = -1$ which implies a constant aspect ratio H/R of the disk, where H denotes the vertical pressure scale height of the disk. The radial temperature gradient and the action of gravity by the star results in the following hydrostatic disk configuration for the density

$$\rho(R, Z) = \rho_0 \left(\frac{R}{R_\mathrm{p}}\right)^p \exp\left[\frac{GM_*}{c_\mathrm{s}^2}\left(\frac{1}{r} - \frac{1}{R}\right)\right]$$

and angular velocity

$$\Omega(R, Z) = \Omega_\mathrm{K}\left[(p+q)\left(\frac{H}{R}\right)^2 + (1+q) - \frac{qR}{\sqrt{R^2+Z^2}}\right]^{\frac{1}{2}}$$

In these equations, $M_* = 1M_\odot$, c_s = sound speed, R_p = planet position, $p = -1.5$, Ω_K is the Keplerian angular velocity, and ρ_0 the density at the reference radius, $R_\mathrm{p} = 5.2\,\mathrm{AU}$.

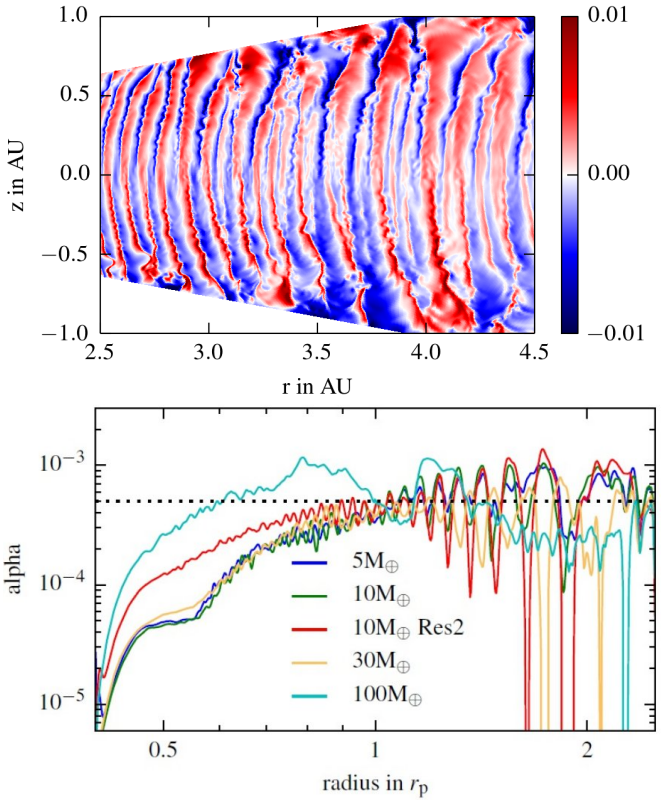

Figure 1. The structure of a VSI-turbulent disk. **Top**: Vertical velocity v_θ (at the $\phi = 0$ slice), red positive, blue negative. In equilibrium state, after a few 100 orbits. Adapted from [7]. **Bottom**: Radial α value for disks for different planet masses. The model labeled 'Res2' has twice the resolution. Adapted from [9].

In this setup we embed planets of different masses and evolve the system in time until a quasi-stationary equilibrium is reached where the turbulence in the disk, driven by the VSI, has saturated. Then we measure the turbulent stresses, quantify the effectiveness of the turbulence, and obtain an effective value of $\alpha = 5 \cdot 10^{-4}$. Using this value for α in a disk setup with explicit viscosity we run comparison simulations to estimate the effect of the turbulence on the embedded planet. The planet is held on a fixed orbit and the torques are measured. The disk section that is modeled extends in radius from $0.4R_\mathrm{p}$ to $2.5R_\mathrm{p}$, where $R_\mathrm{p} = 5.2\,\mathrm{AU}$ is the orbital distance of the planet to the star. Vertically

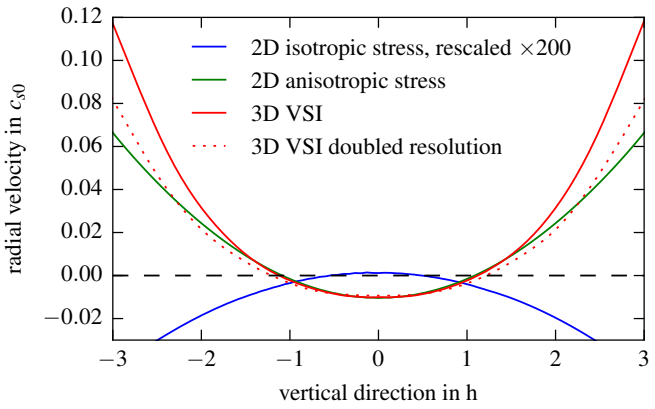

Figure 2. Radial velocity profile, averaged over 50 orbits. Shown are two VSI turbulent disks in 3D simulations in different resolutions, for which the velocity has been azimuthally averaged. The 2D anisotropic model has been calculated for cylindrical coordinates in axisymmetry. The viscous case with isotropic viscosity (standard α-disk) has been rescaled to better visualize the difference. Adapted from [8].

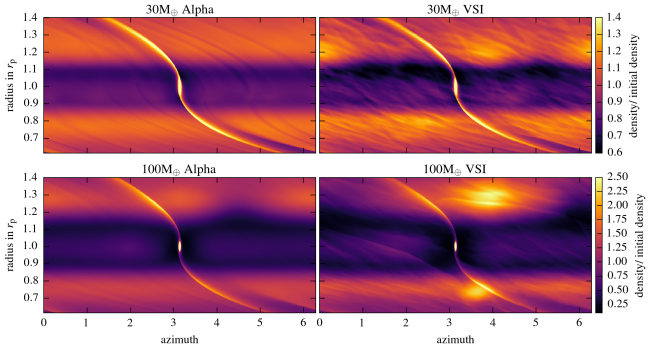

Figure 3. 2D surface density distribution for disks with planets of 30 and 100 $M_\oplus$. **Right**: VSI turbulent disk. **Left**: corresponding viscous disk with $\alpha = 5 \cdot 10^{-4}$. Adapted from [9].

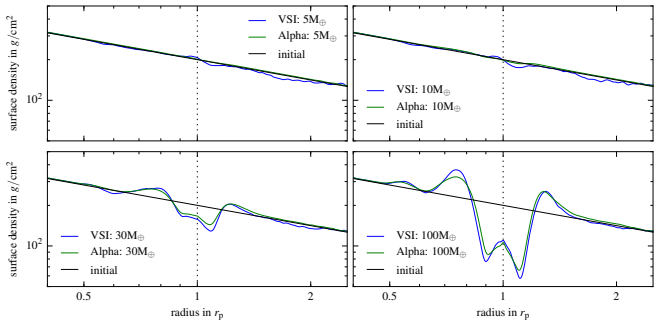

Figure 4. Radial surface density profile for the 4 different planets after 200 orbits. Shown are the profiles for the VSI disk (in blue), the corresponding α-disk (in green) and the initial profile (in black). Adapted from [9].

the disk section covers 5 pressure scale heights, H, above and below the equator, and a full annulus $[0, 2\pi]$ in the azimuthal direction. This computational domain is covered with $N_r = 600, N_\theta = 128$, and $N_\phi = 1024$ gridcells that are spaced logarithmically in the radial and equidistant in the other two directions. We ran a comparison model where we doubled the spatial resolution, to check convergence of the results on α.

II. The turbulent disk

The structure of the VSI-turbulent disk with locally isothermal background is displayed in Fig. 1. The vertical velocity is shown in the top panel in the central (radial) part of the disk. The turbulent elements stretch over the complete vertical direction and show signs of Kelvin-Helmholtz instabilities between upward and downward motions. The effective α-value is plotted in the lower panel where the radial distribution, $\alpha(r)$, is plotted for various planet masses. To estimate the α-parameter as a function of the radius we first calculate the Reynolds stress in cylindrical coordinates (R, Z, ϕ)

$$R_{R,\phi} = \rho u_R \delta u_\phi \,, \tag{1}$$

where u_R is the radial velocity and δu_ϕ is the deviation of the azimuthal velocity from its mean. The α-value is obtained by

$$\alpha(r) = \frac{\langle R_{R,\phi} \rangle_{t,\theta,\phi}}{\langle P \rangle_{t,\theta,\phi}} \,, \tag{2}$$

where P is the pressure and $\langle\rangle_{t,\theta,\phi}$ denotes the average over time, here 140 orbits of the planet, and a spatial average over the whole vertical and azimuthal domain.

The average value found in our simulations lies at $\alpha = 5 \cdot 10^{-4}$ (bottom panel in Fig. 1), relatively independent of the planet mass, where the planet is located at $r = 1$. In the inner parts of the disk the effective α is lower, partly because the inner regions are damped for stability reasons with an explicitly added viscosity. The model with twice the spatial resolution yields the same α-value.

In Fig. 2 we display the mean radial velocity profile for the turbulent and laminar disk as a function of vertical distance. Surprisingly, the radial flow within the disk is directed inwards near the midplane of the disk and outward near the surface layers. This behaviour is exactly opposite to what is seen in laminar viscous disks, as shown by the blue (scaled) curve. In [8] we show that this opposite flow structure is a direct consequence of an anisotropic turbulence, where the $Z - \phi$ component of the turbulent stress tensor is much larger than the $R - \phi$ part, see also [6].

III. The density distribution

Having calculated the efficiency of the VSI-turbulence, we ran comparison models for viscous disks using exactly this α-value. In Fig. 3 we compare the resulting 2D surface density structure (obtained by integrating the density vertically over the disk) of the VSI turbulent case with the corresponding α-disks. Shown is the configuration near the end of the simulations after about 200 orbits of the planet. One notices that for the VSI disk vortices are visible at the outer and inner edge of the gap. These are created by the action of the planet in an inviscid disk. For the 30 $M_\oplus$ case there are two relatively weak vortices visible on either side of the planet. For the more

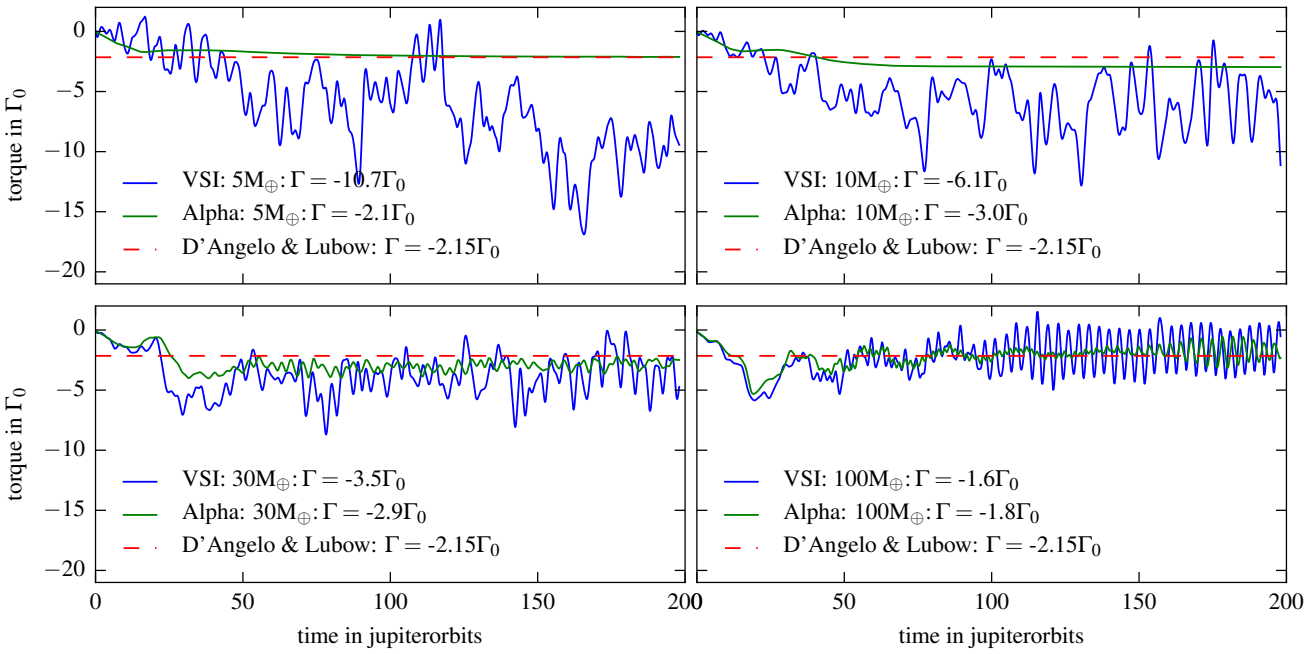

Figure 5. Time evolution of the total torque acting on the planets of different mass. Blue: VSI model, green: corresponding α disk, red dashed: results of [1] for low mass planets. The quoted torque values are averaged over the last 50 orbits of the simulations. Adapted from [9].

massive planet there is only one single vortex remaining on each side.

In Fig. 4 we compare the radial surface density distributions, obtained by additional averaging over the azimuthal direction. Clearly, the gap structure of VSI- and α-disk agree very well with each other. This is an additional indication that the radial angular momentum transport generated by the turbulence can be captured nicely by a corresponding viscous flow using an appropriate value for the effective viscosity.

IV. The torques acting on the planets

The time evolution over the last 50 orbits of the total torque acting on the planets with different masses is shown in Fig. 5. Displayed is the torque evolution for the VSI turbulent disk (blue), and the laminar α-disk (green). We compare our results to the studies by [1] and we normalize the total torque to

$$\Gamma_0 = \Sigma(R_\mathrm{p})\Omega^2(R_\mathrm{p})R_\mathrm{p}^4\left(\frac{M_\mathrm{p}}{M_*}\right)^2\left(\frac{R_\mathrm{p}}{H}\right)^2, \qquad (3)$$

where M_* denotes the mass of the central star. The torques acting on the planets in the viscous disk are significantly smoother than those in the turbulent disk, and they match the findings of previous studies [1] very well. Those were obtained for low mass planets in the linear regime and hence the normalized values all agree. The torques for the larger planets (30, 100 $M_\oplus$) agree well with the expectation but the values for the smaller masses are on average more negative that the laminar values which leads to a faster inward migration towards the central star. The results come about because in the turbulent disk case there is *on average* a density enhancement just inside and behind the planet, creating a negative torque

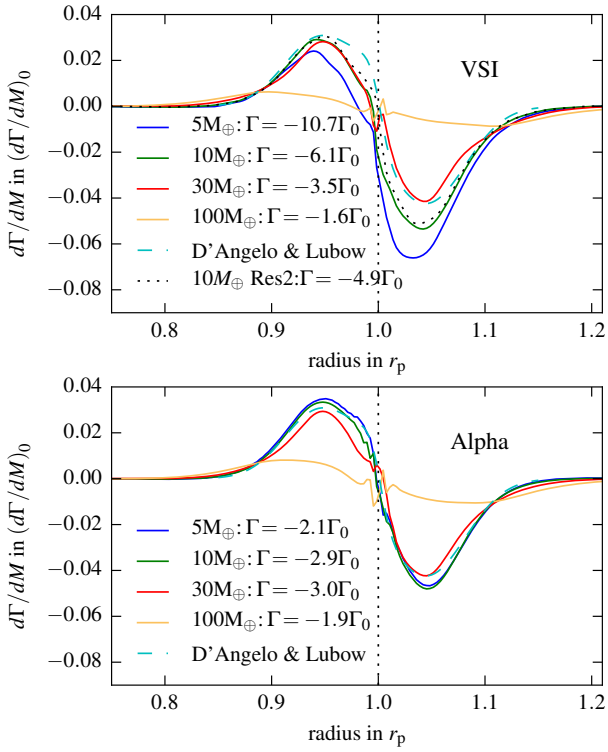

Figure 6. Radial torque density for planets of different masses for the VSI case (top) and α-disk (bottom), averaged over the last 50 orbits. For comparison the analytic profile, that has been obtained by fitting numerical results by D'Angelo & Lubow (2010) [1], is shown. The label Res2 refers to a model with double spatial resolution. Adapted from [9].

contribution. For larger planet masses this density structure is no longer visible. The stochastic fluctuations (in the first 3 panels for the lower masses) are due to the turbulent motions in the disk. These are typically smaller than those found in MRI-turbulent disks as the turbulence is more vigorous in ideal MHD simulations, where they can be much larger than the mean values leading to extended phases of outward migration [5], [10]. The very regular variations in last panel ($100 M_\oplus$ planet) resembles the beat period with the outer vortex (see Fig. 3, bottom right). The torque average over the last 50 orbits is quoted in the legend for each of the four cases.

To analyse our results further, we study the radial distribution of the torque density, which we express in units of

$$\left(\frac{d\Gamma}{dm}\right)_0 = \Omega^2(R_\mathrm{p}) R_\mathrm{p}^2 \left(\frac{M_\mathrm{p}}{M_s}\right)^2 \left(\frac{R_\mathrm{p}}{H}\right)^4 . \qquad (4)$$

The radial torque density is defined such that the total torque is given by the integral over all contributions of the disk

$$\Gamma_\mathrm{tot} = 2\pi \int_\mathrm{disk} \frac{d\Gamma}{dm} \Sigma r dr \, . \qquad (5)$$

The results are displayed in Fig. 6 for the VSI disk (top) and α-disk (bottom). All model show the generic feature of the Lindblad torques where inside of the planet the torque density is positive and outside negative. This structure is created by the action of the two spiral arms originating at the planet location, see Fig. 3. For the laminar α-disk (lower panel) the normalized torque densities agree very well with the linear expectation of [1], while for the 100 $M_\oplus$ planet the onset of gap formation reduced the torques next to the planet, but in such a way to maintain approximately the same total torque as seen above. For the turbulent disk (upper panel) the torque density changes such that inside of the planet the torque is less positive while on the outer disk the torque is more negative. This leads altogether to a significantly increased inward migration speed for the two smaller planets, while the massive planets migrate at approximately the speed that is expected. This is indicated by the quoted total torques, Γ, that are obtained by integrating the individual components of each cell over the whole disk, see eq. (5).

V. Summary

In this work we have studied the interaction of embedded planets in turbulent disk driven by the vertical shear instability (VSI). For the analysed masses (ranging from 5 to 100 $M_\oplus$) the planets have only a very limited effect on the turbulence level in the disk. In our locally isothermal models with $H/R = 0.05$ the angular momentum transport created by the VSI corresponds to an effective turbulent viscosity $\alpha = 5 \cdot 10^{-4}$. Low mass planets have only a small impact on the disk surface density but planets more massive than about 10 $M_\oplus$ begin to carve gaps in the disk. The gap edges become unstable to the Rossby wave instability and vortices develop. Starting from several smaller vortices in the initial phase, eventually they merge to one large vortex one on each side of the planet. The lifetime of the vortices is much longer in the VSI-active disk due to vorticity perturbations generated by the VSI.

For planets with masses smaller than about $10 M_\oplus$ the time averaged torques are negative throughout. For the lowest mass we find inward migration which is about 5 times faster than for the corresponding α-disk model. This effect is due to a density bump behind the planet, that becomes noticeable in the time averaged surface density distribution. From our results we can infer that inviscid disks will generate turbulence driven by the VSI with a finite turbulence level. Hence in realistic 3D discs, the depth of the gap created by the planet is limited, such that planet migration will always occur. We do not expect that planets will stall, even in inviscid disks, as has been suggested for example by [2].

VI. HPC Resources

The simulations for this project were performed in the vast majority on the ForHLR-I high performance computer system installed at the Steinbuch Centre for Computing (SCC) in Karlsruhe. For the simulations the 3D hydrodynamic code `PLUTO` [4] was applied using MPI-parallization. Each run used 400 processors (20 processors per node and 20 nodes). They lasted on average 7 days and used in total 67200 core hours per different run

Acknowledgments

The authors acknowledge support by the High Performance and Cloud Computing Group at the Zentrum für Datenverarbeitung of the University of Tübingen, the state of Baden-Württemberg through bwHPC and the German Research Foundation ("Deutsche Forschungsgemeinschaft", DFG) through grant no INST 37/935-1 FUGG. G. Picogna acknowledges the support through the DFG grant KL 650/21. M.H.R. Stoll received financial support from the Landesgraduiertenförderung of the state of Baden-Württemberg, and acknowledges support through DFG grant KL 650/16. The plots in this publication have been made by the use of the matplotlib package by [3].

References

[1] G. D'Angelo and S. H. Lubow, "Three-dimensional Disk-Planet Torques in a Locally Isothermal Disk," *ApJ*, vol. 724, pp. 730–747, Nov. 2010.
[2] J. Fung and E. Chiang, "Save the Planet, Feed the Star: How Super-Earths Survive Migration and Drive Disk Accretion," *ApJ*, vol. 839, p. 100, Apr. 2017.
[3] J. D. Hunter, "Matplotlib: A 2d graphics environment," *Computing In Science & Engineering*, vol. 9, no. 3, pp. 90–95, 2007.
[4] A. Mignone, G. Bodo, S. Massaglia, T. Matsakos, O. Tesileanu, C. Zanni, and A. Ferrari, "PLUTO: A Numerical Code for Computational Astrophysics," *ApJS*, vol. 170, pp. 228–242, May 2007.
[5] R. P. Nelson, "On the orbital evolution of low mass protoplanets in turbulent, magnetised disks," *A&A*, vol. 443, pp. 1067–1085, Dec. 2005.
[6] A. A. Philippov and R. R. Rafikov, "Radial Transport and Meridional Circulation in Accretion Disks," *ApJ*, vol. 837, p. 101, Mar. 2017.
[7] M. H. R. Stoll and W. Kley, "Vertical shear instability in accretion disc models with radiation transport," *A&A*, vol. 572, p. A77, Dec. 2014.
[8] M. H. R. Stoll, W. Kley, and G. Picogna, "Anisotropic hydrodynamic turbulence in accretion disks," *A&A*, vol. 599, p. L6, Mar. 2017.
[9] M. H. R. Stoll, G. Picogna, and W. Kley, "Planet-disc interaction in laminar and turbulent discs," *A&A*, vol. 604, p. A28, Jul. 2017.
[10] A. L. Uribe, H. Klahr, M. Flock, and T. Henning, "Three-dimensional Magnetohydrodynamic Simulations of Planet Migration in Turbulent Stratified Disks," *ApJ*, vol. 736, p. 85, Aug. 2011.